第 33 卷第 8 期
2017 年 8 月

无 机 化 学 学 报
CHINESE JOURNAL OF INORGANIC CHEMISTRY

Vol.33 No.8
1330-1338

# 金属有机框架材料对[Fe(HB(pz)$_3$)$_2$]自旋转换行为的影响

赵 田*,[1] Ishtvan Boldo[2] Christoph Janiak*,[2] 刘跃军[1]

([1]湖南工业大学包装与材料工程学院,先进包装材料与技术湖南省重点实验室,株洲 412007)

([2]德国杜塞尔多夫大学无机化学与结构化学研究所,杜塞尔多夫 D-40225)

**摘要**:通过在介孔结构金属有机框架材料 MIL-101(Cr)和 MIL-100(Al)的孔洞中合成自旋交叉化合物[Fe(HB(pz)$_3$)$_2$]的方法,可以得到 SCO@MOF 复合物。通过红外光谱(FTIR)、粉末 X 射线衍射(PXRD)、原子吸收光谱(AAS)以及气体吸附-脱附等进行了进一步测试。通过变温磁测量对复合材料的温度诱导自旋转换行为的研究表明,复合材料的自旋转换行为发生改变甚至是消失了。复合材料的这一现象可以解释为[Fe(HB(pz)$_3$)$_2$]在 MOF 主体材料的孔洞中形成了一种新的结晶相,且孔壁压力将会阻碍[Fe(HB(pz)$_3$)$_2$]从低自旋态向高自旋态转变。不同 SCO@MOF 复合物得到了相似的自旋转换行为结果。这确认了当自旋交叉化合物在金属有机框架材料孔洞中形成时,MOFs 材料的限制压力或基体效应对其自旋转换行为的影响显然是至关重要的。

**关键词**:自选交叉化合物; [Fe(HB(pz)$_3$)$_2$]; 金属有机框架材料; 基体效应

**中图分类号**:O614.61$^+$1; O614.3$^+$1; O614.81$^+$1 **文献标识码**:A **文章编号**:1001-4861(2017)08-1330-09

**DOI**:10.11862/CJIC.2017.178

## Effect of Metal-Organic Frameworks on the Spin-Transition Behavior of [Fe(HB(pz)$_3$)$_2$]

ZHAO Tian*,[1] Ishtvan Boldog[2] Christoph Janiak*,[2] LIU Yue-Jun[1]

([1]*Key Laboratory of Advanced Packaging Materials and Technology of Hunan Province, School of Packaging and Materials Engineering, Hunan University of Technology, Zhuzhou, Hunan* 412007, *China*)

([2]*Institute of Inorganic Chemistry and Structural Chemistry, University Düsseldorf, Universitätsstr.* 1 40225 *Düsseldorf, Germany*)

**Abstract:** The spin-crossover (SCO) compound [Fe(HB(pz)$_3$)$_2$] was synthesized in the pores of mesostructured metal-organic frameworks MIL-101(Cr) and MIL-100(Al) to yield SCO@MOF composites as evidenced by infrared spectrometry (FTIR), powder X-ray diffractometry (PXRD), atomic absorption (AAS) and gas adsorption-desorption studies. Studies of the temperature-induced spin crossover behavior of the composites by temperature-variable magnetic measurements of the composites indicate that the spin transitions of the composites are changed (TZ-SP-1) or disappeared (TZ-SP-2). The effect for SCO@MOF composites may be explained with formation of new crystalline phase of [Fe(HB(pz)$_3$)$_2$] in the pores of MOF host materials and the pore wall pressure of MOFs prevent the transition of [Fe(HB(pz)$_3$)$_2$] from low-spin state to high-spin state. The similar SCO behaviour of [Fe(HB(pz)$_3$)$_2$] for different SCO@MOF composites confirms that the confinement pressure or matrix effect on the spin transition is apparently crucial when the SCO compound is formed in the pores of metal-organic frameworks.

**Keywords:** spin-crossover compound; [Fe(HB(pz)$_3$)$_2$]; metal-organic frameworks; matrix effect

收稿日期:2017-04-13。收修改稿日期:2017-06-27。

国家自然科学基金(No.11372108)和德国联邦教育与研究部(No.03SF0492C)资助项目。

*通信联系人。E-mail:tian_zhao@hut.edu.cn,janiak@uni-duesseldorf.de

## 0 Introduction

Spin crossover, sometimes referred to as spin transition or spin equilibrium, in molecules refers to a change in the magnetic spin state in response to some external stimulus. The effect was first found by Cambi et al. in the early 1930s[1-2], but the systematic study of the spin crossover phenomenon began in the 1960s with the discovery of $Fe(phen)_2(NCS)_2$ (phen=1,10-phenanthroline)[3]. This phenomenon is commonly observed with some first row transition metal complexes with a $d^4$~$d^7$ electron configuration in octahedral ligand geometry[4-5]. For example, for octahedral iron(Ⅱ), there are diamagnetic low spin (LS) state and high spin (HS) state with 4 unpaired electrons. The LS state is enthalpically favored whereas the HS state is entropically favored. SCO occurs when a perturbation causes a switch in spin state HS ⇌ LS[6-8]. Hence the spin state is very easily monitored by a magnetometer.

The reversible switching between the low and high spin states (LS ⇌ HS) is associated with pronounced change of not only the magnetic state from diamagnetic to paramagnetic ($^1A_1$ ($S$=0) ⇌ $^5T_2$ ($S$=2)), but also many other important physical parameters, including optical, structural and dielectric properties. The simplicity of detection of optical (usually LS-red ⇌ HS-yellow and magnetic changes) made the iron(Ⅱ) SCO compounds as early prototypes for information storage[9-10] and sensors[11-12].

The SCO transition can be triggered by change of temperature, pressure, magnetic field, light irradiation (LIESST), or action of a chemical agent (chemo-switching)[13-14]. Production of functional, individually addressable, SCO units[15-16] as small as possible is an important problem actively researched in the area of SCO nanomaterials[17-19]. Various methods for synthesis of SCO nanoparticles[20-22] and thin films[23-24] including nanopatterned[25] growth were successfully implemented, also as prototypal functional elements for nanodevices[26]. One of the traditional problematics of such studies is the problem of loss of abruptness in thermal- and pressure- induced SCO, which is associated with loss of cooperativity, *i.e.* elastic interactions in the solid-state propagating the effect of structural changes during the transition.

One promising possibility is to sacrifice entirely the traditional cooperativity for the possibility of embedding isolated molecular SCO entities in a regular matrix with a precise spatial placement/addressability. A transparent matrix, penetrable for small molecules, but encapsulating the SCO entities should allow light- and chemo-switching, also providing good mechanical protection. The effect of matrix confinement imposing additional elastic interactions between the host and the embedded object is well known for SCO nanoparticles, represented by, either "soft" matrices, like organic polymers, *e.g.* PVP or chitosan, or "hard" ones, realized mainly as core-shell particles. In practically all those cases the matrix is firmly adjoined to the surface of the embedded objects, completely isolating them. However, recently we have observed that in $[Fe(Htrz)_3](BF_4)_2\cdot xH_2O$@MCM-41 the mesoporous zeolite matrix loosely surrounding the embedded 1D SCO polymer could transfer the confinement pressure through absorbed water molecules as mediators, significantly altering the SCO parameters[27]. While in [Fe(HB(pz)$_3$)$_2$]@$NH_2$-MIL101(Al) encapsulation products, the spin transition curves of composites shifted to much lower temperatures and became more gradual(vs bulk[Fe(HB(pz)$_3$)$_2$])[28].

Metal-organic frameworks (MOFs) receive great attention, due to their intriguing structural properties such as high porosity and high thermal stability, which led to many potential applications[29-33]. Some metal particles could be directly formed in the pores of MOFs by reduction of the metal salt. For instance, Pd and Cu particles could be embedded in the pores of MIL-101(Cr) by this method without observed degradation of MOF[34]. In this work, we synthesized the well-studied SCO compound [Fe(HB(pz)$_3$)$_2$] (pz= pyrazolyl, Scheme 1) directly in the pores of two large porosity, stable, well investigated MOFs, MIL-101(Cr) and MIL-100(Al). The MOFs matrix effect, that is, the change in SCO behavior under the constraints of surrounding rigid porous matrix has been studied herein by temperature-variable magnetic measurements.

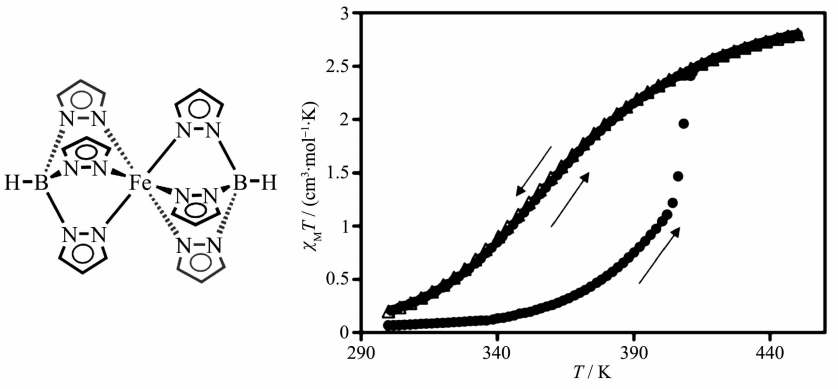


First cycle: closed circles, second cycle: open triangles

Scheme 1 Schematic drawings of SCO material $[Fe(HB(pz)_3)_2]$ and the temperature dependence of the $\chi_M T$ product of $[Fe(HB(pz)_3)_2]$ upon two successive thermal cycles[37]

## 1 Experimental

### 1.1 Synthesis and purification of MIL-101(Cr)

MIL-101(Cr) was synthesized according to the previously reported procedure[35]. A typical synthesis involved a solution containing chromium (Ⅲ) nitrate nonahydrate ($Cr(NO_3)_3\cdot 9H_2O$, 400 mg, 1.0 mmol), nitric acid (1.0 mmol) and terephthalic acid ($H_2BDC$, 166 mg, 1.0 mmol) in 5 mL $H_2O$ with stirring for 10 min. Then the mixture was transferred to the Teflon line in a hydrothermal autoclave which is heated for 8 h at 220 ℃ and cooled afterwards slowly to room temperature at a rate of 30 ℃·h$^{-1}$ in 6 h. The mixture was then isolated from the autoclave and the solid separated from the solution through centrifugation (4 200 r·min$^{-1}$ for 50 min). The contents of autoclave were transferred to two centrifugal tubes and the supernatant solution was carefully removed after centrifugation. Then water (5 mL) was added in each tube and the solid was evenly dispersed in the aqueous phase. After renewed centrifugation and removal of the supernatant solution, DMF (5 mL) was added to each tube which was placed in a hot (80 ℃) ultrasonic bath and sonicated for 1 h. Centrifugation was again used to separate MIL-101 and DMF. The precipitate was transferred in a 25 mL beaker where it was stirred with 10 mL of water at room temperature for 5 h. After separation by centrifugation, the same washing procedure but using ethanol was repeated once more at the same temperature. The final product was obtained by centrifugation and dried in a vacuum oven (100 ℃, 1 200 Pa) for 2 h.

### 1.2 Synthesis and purification of MIL-100(Al)

Aluminium-based MIL-100 trimesate ($Al_3O(OH)(H_2O)_2[btc]_2\cdot nH_2O$) was synthesized according to the previously reported procedure[36]. A typical synthesis involved a solution containing aluminium (Ⅲ) nitrate hexahydrate ($Al(NO_3)_3\cdot 6H_2O$, 230 mg, 0.61 mmol), nitric acid (0.77 mmol) and trimethyl 1,3,5-benzenetricarboxylate ($btcMe_3$, 104 mg, 0.41 mmol) in 2.8 mL $H_2O$. Then the mixture was transferred to the Teflon line in a hydrothermal autoclave which is heated for 3.5 h at 210 ℃ (the temperature went up to 210 ℃ in 1 h) and cooled afterwards slowly to room temperature at a rate of 30 ℃·h$^{-1}$ in 6 h. The resulting yellowish powdered sample was collected by filtration, washed with water, and dried at room temperature for overnight. Then the collected solid and 10 mL DMF were transferred to a 20 mL Parr-type Teflon-lined autoclave and heated at 150 ℃ for 4 h. The mixture was then isolated from the autoclave and the solid separated by filtration, washed with water, and dried at room temperature for overnight. After that, the white powdered product was washed with water in reflux at 100 ℃ for 12 h and then collected by filtration at room temperature. The product was placed at ambient condition for 12 h and then stored in a glass bottle.

### 1.3 Synthesis of $[Fe(HB(pz)_3)_2]$ in the pores of MOFs

Host MOF material (50 mg) was added to a

solution of potassium tri(1-pyrazolyl) borohydride (126 mg, 0.5 mmol, in 5 mL $H_2O$) with stirring at room temperature for 12 h. Then a solution of ammonium iron(Ⅱ) sulfate hexahydrate (98 mg, 0.25 mmol, in 5 mL $H_2O$) was added to this solution and with stirring at room temperature for another 2 days. The precipitate was isolated by centrifugation (4 200 r·min$^{-1}$ for 10 min) and washed with dichloromethane for three times to remove the residues of [Fe(HB(pz)$_3$)$_2$] outside of the pores of MOF. Centrifugation was used to separate solid sample and dichloromethane. The precipitate was transferred in a 25 mL beaker and stirred with 10 mL of water at 70 ℃ for 5 h. After separation by centrifugation, the final product was dried in the vacuum oven (100 ℃, 1 200 Pa) for 2 h.

### 1.4 Sample characterization

Powder X-ray diffraction (PXRD) measurements were carried out with a Bruker D2 Phaser using a flat silicon, low background sample holder and Cu $K\alpha$ radiation ($\lambda$=0.154 184 nm) at 40 mA, 30 kV ($2\theta$=7°~50°). Diffraction patterns were obtained on flat layer sample holders where at low angle the beam spot is strongly broadened so that only a fraction of the reflected radiation reaches the detector which leads to the low relative intensities measured at $2\theta$<7°.

Nitrogen physisorption isotherms at 77 K were obtained using a NOVA-4000e instrument within a partial pressure range of $10^{-6}$~1.0. The samples were degassed under high vacuum ($1.33\times10^{-3}$ Pa) at 120 ℃ for at least 2 h, prior to each measurement. The BET surface areas were calculated from adsorption isotherm data points in the pressure range $p/p_0$=0.05~0.2.

Infrared spectra (IR) were measured on a Bruker Tensor 37 FT-IR Spectrometer with ATR disks.

Atom absorption spectroscopy (AAS) was conducted with a Perkin Elmer AAnalyst100 instrument (AAS flame: acetylene/air flame, burner head length: 10 cm). The standard solution were prepared with densities of 1, 5 and 10 mg·L$^{-1}$, respectively. The iron content of each sample was determined by the comparison of standard solution.

DC magnetic measurements were performed by using Quantum Design MPMS XL-5 SQUID magnetometer. For both samples, $M(T)$ measurements were carried out in the magnetic field of 1 000 Oe, starting from 5 to 400 K (heating), and then cooling back to 200 K.

Elemental (C, H, N) analysis was done with a Perkin-Elmer Series 2 Elemental Analyser 2400.

## 2 Results and discussion

MIL-101(Cr) and MIL-100(Al) were used as host materials in this work, the corresponded samples were named as TZ-SP-1 and TZ-SP-2 respectively. Due to the presence of [Fe(HB(pz)$_3$)$_2$], the changing of colour would be expected. In fact, TZ-SP-1 was a kind of grey powdered solid, while TZ-SP-2 was pale orange powder (Fig.1).

Comparison of the IR spectra of the TZ-SP samples with both bulk MOFs and bulk [Fe(HB(pz)$_3$)$_2$] confirms encapsulation (Fig.2). For TZ-SP samples, the main difference of IR patterns falls in the fingerprint region from 1 000 to 1 200 cm$^{-1}$. There is a clear evidence of the presence of the iron complex in the

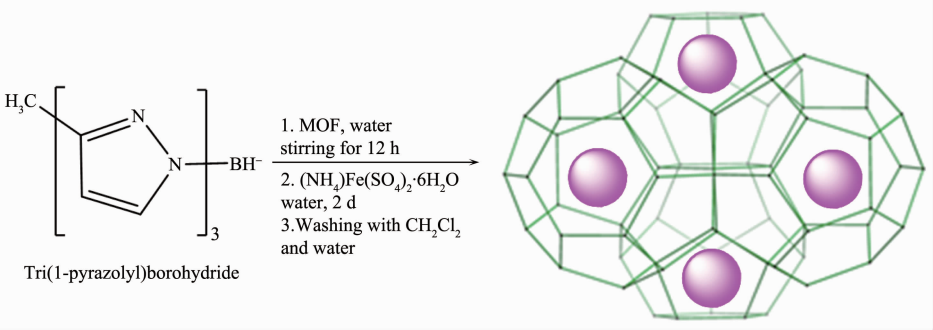


Pink ball: [Fe(HB(pz)$_3$)$_2$] molecule

Scheme 2　Schematic drawing of synthesis of [Fe(HB(pz)$_3$)$_2$] in the pores of MOFs

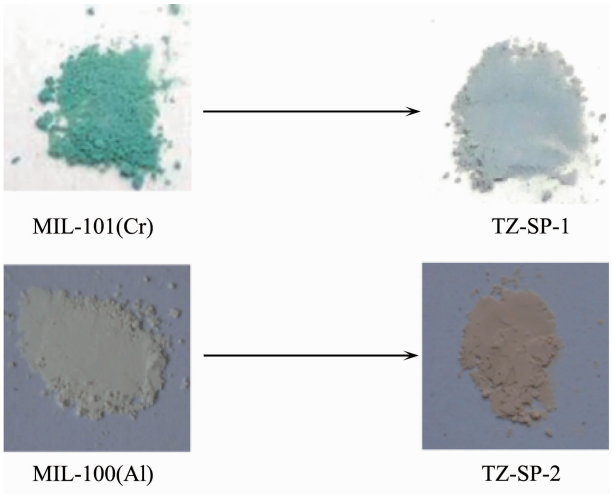


Fig.1 Comparison of colour of TZ-SP sample with that of corresponded MOF

TZ-SP encapsulation product compared to the non-loaded MIL matrix. In all encapsulated products the two main peaks of the bulk $[Fe(HB(pz)_3)_2]$, found at 1 041 $cm^{-1}$ and 1 109 $cm^{-1}$, are slightly shifted to lower frequencies (typically 1 021 and 1 098 $cm^{-1}$) (Fig.2). This low frequency shift may reflect the presence of the weak interactions of the bond moiety with the surroundings, e.g. carboxylate weak H-bond acceptors or residual solvent molecules.

The inclusion of $[Fe(HB(pz)_3)_2]$ in the pores of MIL-101(Cr) and MIL-100(Al) were proven by the analysis on iron and pore size analysis. The iron content determined by atomic absorption spectrometry (AAS) and CHN elemental analysis for N are given in Table 1.

For a better understanding of the actually observed incorporation values, it is expedient to estimate the physically maximal loading, based on the comparison of molecular and pore volumes. From the molecular dimensions of the molecule, approximated as a cylinder (Fig.3b), the van der Waals surface limited molecular volume of 0.357 $nm^3$ can be estimated (Fig. 3). On the other hand, the unit cell volume of 2.158 $nm^3$ of one of the single-crystal X-ray structures of $[Fe(HB(pz)_3)_2]$ with $Z$=4 (Refcode HPZBFE03)[37] gives ~0.540 $nm^3$ volume per single $[Fe(HB(pz)_3)_2]$ molecule at $\rho$=1.483 $g\cdot cm^{-3}$ (Fig.3). The ratio of 0.357/0.540= 0.66 is in the range of typical packing coefficients ($k$= 0.65~0.77) for molecular structures[38].

Taking the known density of the bulk Fe complex, 1.483 $g\cdot cm^{-3}$ as a realistic density estimate for closely packed molecules in the pores, the maximal loading could be estimated as $V_{pore}\cdot\rho$, where $V_{pore}$ is the specific pore volume. The latter could be

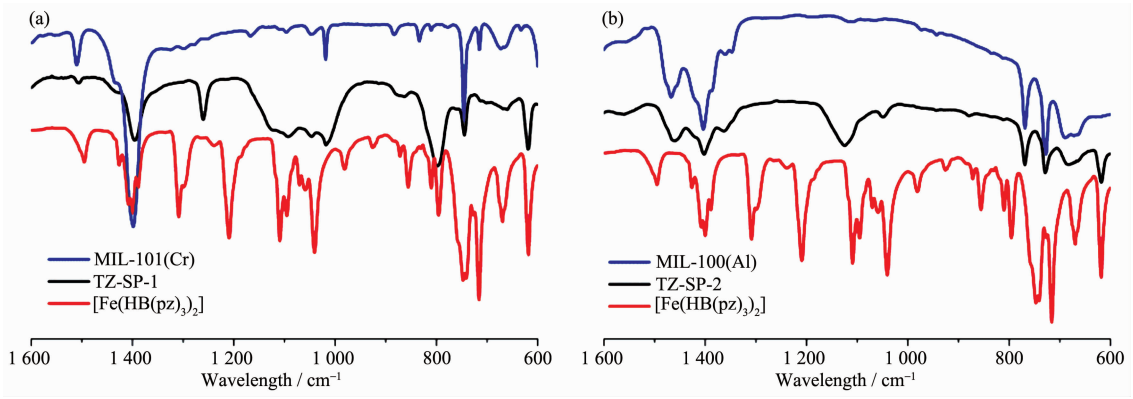


Fig.2 IR spectra of TZ-SP-1 (a) and TZ-SP-2 (b) in comparison to corresponding host MOFs and $[Fe(HB(pz)_3)_2]$

**Table 1 Content(mass fraction) of $[Fe(HB(pz)_3)_2]$ in the TZ-SP samples[a]**

| Sample | Fe content by AAS / % | | $[Fe(HB(pz)_3)_2]$ content / %[b] | | N content by CHN analysis / % | |
|---|---|---|---|---|---|---|
| | Calcd. | Exp. | Calcd. | Exp. | Calcd.[c] | Exp. |
| TZ-SP-1 | 1.71 | 1.66[d] | 14.76 | 14.32[d] | 5.15 | 5.67[d] |
| TZ-SP-2 | 1.17 | 1.21[d] | 10.10 | 10.44[d] | 3.52 | 3.81[d] |

[a] Each sample was dried in the vacuum oven (120 ℃, 1 200 Pa) for 2 h before AAS analysis; [b] Fe content in $[Fe(HB(pz)_3)_2]$, $C_{18}H_{20}B_2N_{12}Fe$ ($M_r$=481.91) is 11.59%; [c] Calculated value of N were obtained based on the AAS analysis results; [d] Fe analysis after the samples were dried at 120 ℃ and $1.33\times10^3$ Pa for an additional 4 h.

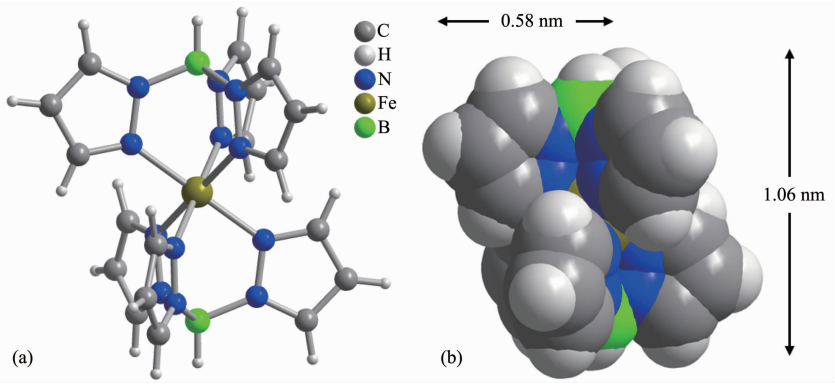


Fig.3　Structure of [Fe(HB(pz)$_3$)$_2$] (Refcode HPZBFE03)[37]: (a) ball-and-stick presentation; (b) space-filling presentation of single molecule

estimated at 1.56 cm$^3$·g$^{-1}$ for MIL-101(Cr) and 0.75 cm$^3$·g$^{-1}$ for MIL-100 (Al) from the value of gas uptake based total pore volume of 1.16 cm$^3$·g$^{-1}$ for MIL-101 (Cr) and 0.80 cm$^3$·g$^{-1}$ for MIL-100 (Al), saving 0.10 and 0.05 cm$^3$·g$^{-1}$, respectively, part associated with pores with $d$<1 nm as estimated by NL-DFT model. Hence, the maximum loading for MIL-101(Cr) is 1.483 g·cm$^{-3}$×1.56 cm$^3$·g$^{-1}$=2.31 $g_{Fe\text{-}complex}$·$g_{MIL}^{-1}$, or 2.31/(2.31+1)=~69% by weight. While for MIL-100(Al), the maximum loading is 1.483 g·cm$^{-3}$×0.75 cm$^3$·g$^{-1}$=1.11 $g_{Fe\text{-}complex}$·$g_{MIL}^{-1}$, or 1.11/(1.11+1)≈52% by weight.

The achieved incorporation of ~14% and 10% (Table 1) are, as expected, significantly less than the value estimated above. It is because that the Fe-complex, synthesized in the pores of MILs, and high incorporation rates are not expected, particularly under conditions, where the large molecules of the iron complex is strongly hindered. During the synthesis, the pores are also filled by solvent molecules, ligands molecules and low-molecular coordination-bonded "synthetic debris" and some of those components could also perform an important templating action (*i.e.* the sufficient washing agent DMF might be crucial).

Powder X-ray diffraction (PXRD) measurements of TZ-SP samples show significant change in comparison to their own corresponded MOF host materials (Fig.4). First, all the characterized reflection of MOF host materials could be easily observed in TZ-SP sample, it is disclosed that, the MOFs remained structurally robust after the synthesis procedure. Second, the typical reflection from [Fe(HB(pz)$_3$)$_2$] at 10.07° also can be easily observed in both samples. But, there were two new high reflections at 29.54° and 30.55° in both TZ-SP samples, while the corresponded positions of PXRD pattern of bulk-[Fe

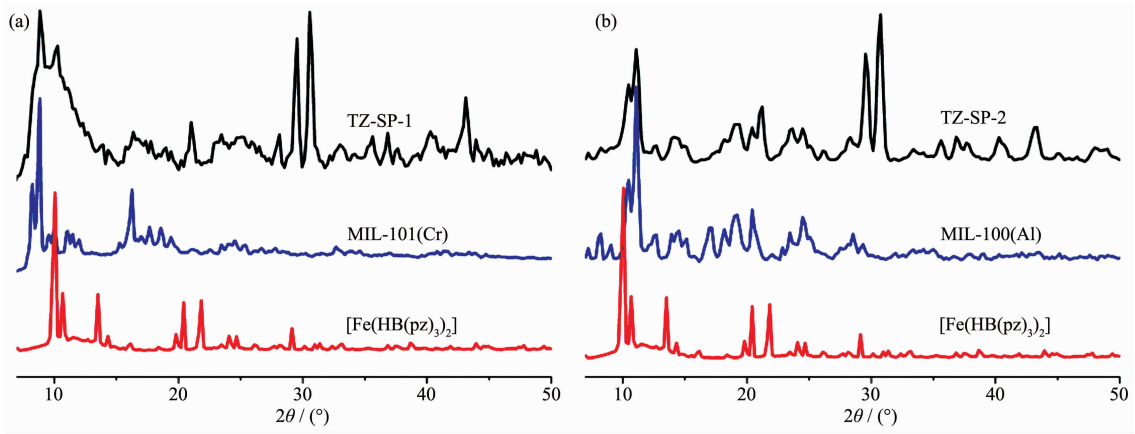


Fig.4　Powder X-ray diffraction patterns of TZ-SP-1(a) and TZ-SP-2 (b) compared with corresponded MOF host materials and [Fe(HB(pz)$_3$)$_2$]

$(HB(pz)_3)_2]$ only possessed a small peak at 29.13°. Meanwhile, for both TZ-SP samples, there were several other observed reflections at 36.84°, 37.65°, 40.29° and 43.13°. These new reflections were not characteristic for bulk $[Fe(HB(pz)_3)_2]$, which indicates that $[Fe(HB(pz)_3)_2]$ forms another crystalline phase in the pores of MOF host materials. In the pores of the regular matrix, $[Fe(HB(pz)_3)_2]$ may be preferred orientations of crystals.

The remaining porosity of the composite materials was analyzed by $N_2$ adsorption-desorption studies at 77 K (Fig.5). The sample was pre-treated before measurement by outgassing under vacuum at 393 K for 2 h. For the composite materials, the Brunauer-Emmett-Teller (BET) and Langmuir surface areas have largely decreased. For TZ-SP-1, only 260 $m^2 \cdot g^{-1}$ of BET surface area had been remained, and it decreased more than 90% compared to MIL-101(Cr). For TZ-SP-2, it possesses only 75 $m^2 \cdot g^{-1}$ of BET surface, which also decreased over 90% than that of MIL-100(Al).

The SCO behavior of bulk $[Fe(HB(pz)_3)_2]$ is well described in the literature[37-40]. Heating a crystalline sample of $[Fe(HB(pz)_3)_2]$, recrystallized from hot toluene[39] or freshly sublimed[37], from room temperature[39] or 90 K[37] to above 400 K results in an increase of effective magnetic moment from <1.0$\mu_B$ to 4.9$\mu_B$ which indicates a change from primarily LS $^1A_{1g}$ to the HS $^5T_{2g}$ state. Yet, this increase is slow and very gradual up to 390 K (~2.90$\mu_B$) at which point a sharp rise in effective magnetic moment to 4.14$\mu_B$ occurs. This sharp increase was assigned to a crystallographic phase transition: the initial well-formed crystals shatter into extremely small fragments. The phase transition is accompanied by a change in the electronic ground state to an essentially high-spin configuration. The magnetic moment reaches the spin-only value of 4.90$\mu_B$ for iron(Ⅱ) at 461 K[39-40]. Upon cooling the same sample shows no sharp decrease in magnetic moment anymore. The decrease occurs gradual to ~1.38$\mu_B$ at 298 K and to 0.61$\mu_B$ at 90 K. During a second heating of the same sample the magnetic moment follows the gradual preceding cooling curve. Thus, the change in magnetic moment or susceptibility displayed a hysteresis only for the first thermal cycle. Subsequent heating and cooling cycles following the first cooling curve and not the first heating curve as the initially

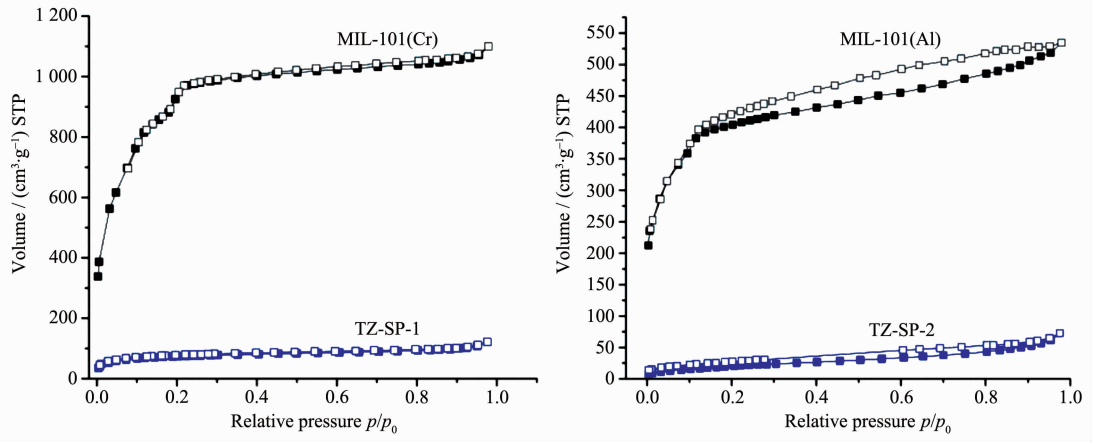


Fig.5 $N_2$ adsorption-desorption isotherms of TZ-SP samples in comparison to corresponded MOFs

**Table 2 Texture properties of TZ-SP samples and the corresponded MOFs**

| Material | $S_{BET}$ / $(m^2 \cdot g^{-1})^a$ | $S_{Langmuir}$ / $(m^2 \cdot g^{-1})$ | $V_{pore}$ / $(cm^3 \cdot g^{-1})^b$ |
|---|---|---|---|
| MIL-101(Cr) | 3 450 | 4 610 | 1.66 |
| TZ-SP-1 | 260 | 350 | 0.17 |
| MIL-100(Al) | 1 450 | 1 880 | 0.80 |
| TZ-SP-2 | 75 | 112 | 0.09 |

[a] Calculated in the pressure range $0.05 < p/p_0 < 0.2$ from $N_2$ sorption isotherm at 77 K with an estimated standard deviation of ± 50 $m^2 \cdot g^{-1}$; [b] Calculated from $N_2$ sorption isotherm at 77 K ($p/p_0$=0.95) for pores with $d \leqslant 20$ nm

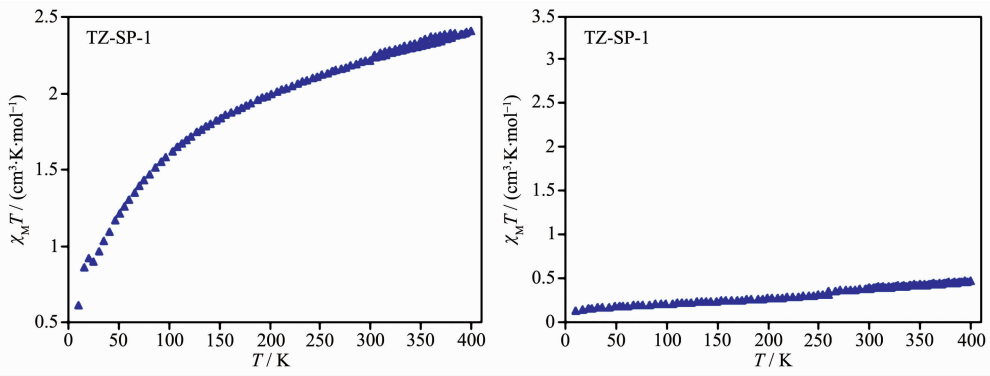


Fig.6　Temperature-variable magnetic curves for TZ-SP-1 and TZ-SP-2

metastable crystalline state of [Fe(HB(pz)$_3$)$_2$] has relaxed into a stable form.

Temperature-variable magnetic curves for the TZ-SPs were monitored using by DC magnetic measurements (Fig.6). Prior to the magnetic measurements the samples were stored under ambient air in a closed glass vessel.

For TZ-SP-1, the transition temperature for [Fe(HB(pz)$_3$)$_2$] has been shifted to much lower values and the spin transition curve became more gradual. This can also be explained by having nano-sized [Fe(HB(pz)$_3$)$_2$] particles in the composite. The smaller the particles of an SCO material, the more gradual the transition and the lower the transition temperature $T_c$. The spin transition of microcrystalline [Fe(pz)Pt(CN)$_4$]·2.6H$_2$O (pz=pyrazine) is much more gradual than bulk material[41]. [Fe(H$_2$Bpz)$_2$(phen)] and [Fe(H$_2$Bpz)$_2$(bipy)] prepared in thin films present a more gradual spin transitions than in the powder samples and shift to lower transition temperature[42]. Though microcrystals of the spin-crossover coordination polymer [FeL(bipy)] (L=[3,3′]-[1,2-phenylenebis(iminoethylidyne)] bis-(2,4-pentanedionato), bipy=4,4′-bipyridine) prepared in a poly(4-vinylpyridine) (P4VP) matrix show the same cooperative spin transition as the bulk material. But the remaining iron centers are either high-spin or low-spin depending on the coordination environment[43]. Furthermore, the temperature variable magnetic susceptibility of TZ-SP-1 shows that, the subsequent cooling curve retraced the heating procedure, which indicates that no crystallographic phase transition occurs due to the matrix confinement of MIL-101(Cr). The similar results are already observed in NH$_2$-MIL-101 (Al), which has the same structure as MIL-101(Cr)[28].

For TZ-SP-2, the spin transition curve shows that, most of Fe(HB(pz)$_3$)$_2$] in the composite still remain in the low-spin state configuration in the whole range of temperature (Fig.6). The $\chi_M T$ value of TZ-SP-2 increases very slowly. Even at 400 K, it is still less than 0.5 cm$^3$·K·mol$^{-1}$. It is because that the HS state has elongated Fe-ligand bond lengths (Fe-N 0.21~0.22 nm) compared to the LS state (Fe-N 0.19~0.20 nm) thereby requiring more space. While the pore size of MIL-100(Al) is much smaller than that of MIL-101(Cr). Thus, the Fe(HB(pz)$_3$)$_2$] confined in the pores of MIL-100(Al) is more difficult to transit from low-spin state to high-spin state. In our previous work, two 1D SCO polymer embedded in the pores of MCM-41 have to operate against the higher pressure exerted by the pore walls of the MCM matrix, which in line with the results[27].

## 3　Conclusions

In conclusion, a well investigated spin-crossover compound [Fe(HB(pz)$_3$)$_2$] have been prepared in the pores of two famous mesostructured metal-organic frameworks MIL-101(Cr) and MIL-100(Al). The identity of TZ-SPs, with loading of iron complex at ~14% and ~10% respectively, were confirmed by PXRD and spectroscopic evidences. The entrapped complex formed another crystalline phase in the pores of MILs. And the transition temperature for [Fe(HB(pz)$_3$)$_2$] in the TZ-SP-1 has been shifted to much lower values and the spin transition curves become more gradual.

For TZ-SP-2, most of $[Fe(HB(pz)_3)_2]$ in the composite still remain in the low-spin state configuration in the whole range of temperature due to higher pressure exerted by the pore walls of MIL-100(Al). Thus, the confinement pressure or matrix effect on the spin transition is apparently crucial when the SCO compound forms in the pores of metal-organic frameworks.

## References:


[1] Cambi L, Cagnasso A. *CI. Sci. Fis. Mat. Nat. Rend.*, **1931**, **13**:809-813

[2] Cambi L, Szego L. *Ber. Dtsch. Chem. Ges. B*, **1931**,**64**:2591-2598

[3] Baker A, Bobonich M. *Inorg. Chem.*, **1964**,**3**:1184-1188

[4] TAO Jian-Qing(陶建清), YU Zhi(余智), SHAO Ting(邵挺), et al. *Chinese J. Inorg. Chem.*(无机化学学报), **2002**,**18**(6):582-586

[5] TAO Jian-Qing(陶建清), SHI Wei-Zhong(施卫忠), ZHUANG Xiao(庄晓), et al. *Chinese J. Inorg. Chem.*(无机化学学报), **2002**,**18**(3):255-258

[6] Brooker S. *Chem. Soc. Rev.*, **2015**,**44**:2880-2892

[7] ZHU Dun-Ru(朱敦如), QI Li(齐丽), CHENG Hui-Min(程慧敏), et al. *Prog. Chem.*(化学进展), **2009**,**21**(6):1187-1198

[8] SHI Hai-Yan(时海燕), WEI Rong-Jia(危荣佳), TAO Jun(陶军). *J. Xiamen Univ.: Nat. Sci.*(厦门大学学报:自然科学版), **2017**,**56**(3):359-363

[9] Kepenekian M, Costa S, Guennic L, et al. *Inorg. Chem.*, **2010**,**49**:11057-11061

[10]Chiruta D, Linares J, Dahoo R, et al. *Physica B*, **2014**,**435**:76-79

[11]Atitoaie A, Tanasa R, Stancu A, et al. *J. Magn. Magn. Mater.*, **2014**,**368**:12-18

[12]Jureschi C, Rusu I, Codjovi E, et al. *Physica B*, **2014**,**449**:47-51

[13]TAO Jian-Qing(陶建清), GU Zhi-Guo(顾志国), WANG Tian-Wei(王天维), et al. *Chinese J. Inorg. Chem.*(无机化学学报), **2005**,**21**(10):1471-1474

[14]TAO Jian-Qing(陶建清), YU Zhi(余智), SHAO Ting(邵挺), et al. *Chinese J. Inorg. Chem.*(无机化学学报), **2003**,**19**(9):1011-1014

[15]Qiu D, Gu L, Sun X L, et al. *RSC Adv.*, **2014**,**4**:61313-61319

[16]Gütlich P, Gaspar A, Garcia Y. *Beilstein J. Org. Chem.*, **2013**,**9**:342-391

[17]Mikolasek M, Félix G, Molnár G, et al. *Phys. Rev. B*, **2014**, **90**:075402

[18]Molnár G, Salmon L, Nicolazzi W, et al. *J. Mater. Chem. C*, **2014**,**2**:1360-1366

[19]Félix G, Nicolazzi W, Salmon L, et al. *Phys. Rev. Lett.*, **2013**, **110**:235-701

[20]Shepherd H, Molnár G, Nicolazzi W, et al. *Eur. J. Inorg. Chem.*, **2013**:653-661

[21]Tissot A, Rechignat L, Bousseksoub A, et al. *J. Mater. Chem.*, **2012**,**22**:3411-3419

[22]Tokarev A, Long J, Guari Y, et al. *New J. Chem.*, **2013**,**37**:3420-3432

[23]Qiu D, Ren D H, Gu L, et al. *RSC Adv.*, **2014**,**4**:31323-31327

[24]Ellingsworth E, Turner B, Szulczewski G. *RSC Adv.*, **2013**, **3**:3745-3754

[25]Basak S, Hui P, Chandrasekar R. *Chem. Mater.*, **2013**,**25**:3408-3413

[26]Dugay J, G-Marqués M, Kozlova T, et al. *Adv. Mater.*, **2015**, **27**:1288-1293

[27]Zhao T, Cuignet L, Dîrtu M, et al. *J. Mater. Chem. C*, **2015**, **3**:7802-7812

[28]Zhao T, Boldog I, Spasojevic V, et al. *J. Mater. Chem. C*, **2016**,**4**:6588-6601

[29]Zhao T, Heering C, Boldog I, et al. *CrystEngComm*, **2017**, **19**:776-780

[30]Jeremias F, Fröhlich D, Janiak C, et al. *RSC Adv.*, **2014**,**4**:24073-24082

[31]HE Zhong-Wen(何仲文), LIU Tao(刘涛), SHI Yao-Qi(石尧麒), et al. *Petrochem. Tech.*(石油化工), **2016**,**45**(9):1094-1099

[32]LI Zhong-Yue(李忠月), LIU Kun(刘昆), ZHANG Yun-Xing(张运兴), et al. *Chinese J. Inorg. Chem.*(无机化学学报), **2012**,***28***(4):710-714

[33]JIANG Jing(江靖), REN Shi-Bin(任世斌), LIN Yong-Qiang(林勇强), et al. *Chinese J. Inorg. Chem.*(无机化学学报), **2013**,**29**(7):1539-1544

[34]Al-Shall M, Abdelsayed V, Khder A, et al. *J. Mater. Chem.*, **2009**,**19**:7625-7631

[35]Zhao T, Jeremias F, Boldog I, et al. *Dalton Trans.*, **2015**,***44***:16791-16801

[36]Volkringer C, Popov D, Loiseau T, et al. *Chem. Mater.*, **2009**,**21**:5695-5697

[37]Salmon L, Molnár G, Cobo S, et al. *New J. Chem.*, **2009**,**33**:1283-1289

[38]Kitaigorodskii A I. *Molecular Crystals and Molecules*. New York: Academic Press, **1973**.

[39]Hutchinson B, Daniels L, Henderson E, et al. *Chem. Commun.*, **1979**:1003-1004

[40]Grandjean F, Long G J, Hutchinson B, et al. *Inorg. Chem.*, **1989**,**28**:4406-4414

[41]Delgado T, Tissot A, Besnard C, et al. *Chem. Eur. J.*, **2015**, **21**:3664-3670

[42]Naggert H, Bannwarth A, Chemnitz S, et al. *Dalton Trans.*, **2011**,**40**:6364-6366

[43]Göbel C, Palamarciuc T, Lochenie C, et al. *Chem. Asian J.*, **2014**,**9**:2232-2238